Optics Letters

Broadband robustly single-mode hollow-core PCF by resonant filtering of higher-order modes

PATRICK UEBEL,* MEHMET C. GÜNENDI, MICHAEL H. FROSZ, GORAN AHMED, NITIN N. EDAVALATH, JEAN-MICHEL MÉNARD, AND PHILIP ST.J. RUSSELL

Max Planck Institute for the Science of Light, G.-Scharowsky-Str. 1/Bldg. 24, 91058 Erlangen, Germany
**Corresponding author: patrick.uebel@mpl.mpg.de*

Received 4 December 2015; revised 16 March 2016; accepted 20 March 2016; posted 21 March 2016 (Doc. ID 255044); published 20 April 2016

We report a hollow-core photonic crystal fiber that is engineered so as to strongly suppress higher-order modes, i.e., to provide robust LP_{01} single-mode guidance in all the wavelength ranges where the fiber guides with low loss. Encircling the core is a single ring of nontouching glass elements whose modes are tailored to ensure resonant phase-matched coupling to higher-order core modes. We show that the resulting modal filtering effect depends on only one dimensionless shape parameter, akin to the well-known d/Λ parameter for endlessly single-mode solid-core PCF. Fabricated fibers show higher-order mode losses some ~100 higher than for the LP_{01} mode, with LP_{01} losses <0.2 dB/m in the near-infrared and a spectral flatness ~1 dB over a >110 THz bandwidth.

OCIS codes: (060.2280) Fiber design and fabrication; (060.2310) Fiber optics; (060.2430) Fibers, single-mode; (060.4005) Microstructured fibers; (060.5295) Photonic crystal fibers.

http://dx.doi.org/10.1364/OL.41.001961

Through their ability to guide light in low-index materials such as gases and liquids, hollow-core photonic crystal fibers (HC-PCFs) provide many opportunities beyond those of solid-core fibers. They are finding applications in high-power beam delivery [1], gas-based nonlinear optics [2], and chemical and gas sensing [3,4]. HC-PCFs typically come in two classes according to their guidance mechanism, i.e., whether it is via a two-dimensional photonic bandgap or antiresonant reflection (ARR) [5].

Several different types of hollow-core ARR-PCFs have emerged in recent years, including fibers with kagomé-style claddings [6] and a new class of simpler structure consisting of a single ring of antiresonant elements (AREs) surrounding a central hollow core [7–10]. These single-ring structures allow faster preform preparation than kagomé or bandgap PCF (because of the lower number of capillaries needed) and, in some cases, offer lower transmission losses, for example, in the mid-IR [11].

Compared to solid-core fibers, in particular, endlessly single-mode (ESM) PCFs [12], a drawback of ARR-PCFs is that they also support a family of higher-order modes (HOMs), i.e., they are not purely single-mode waveguides. Since these HOMs often have relatively low loss, it is very challenging to launch a pure LP_{01} mode without HOM contamination and, even if one succeeds in doing so, HOMs can be excited by bending or external stress, resulting in lower-quality transmitted beam profiles and power fluctuations. This problem is particularly acute in applications using relatively short fiber lengths such as laser machining and pulse compression.

To quantify the degree of HOM suppression, we introduce a figure of merit $FOM_{lm} = \alpha_{lm}/\alpha_{01} - 1$ where α_{lm} is the loss of the LP_{lm} core mode (in dB/m). Applying this FOM to published results, we find that (1) a conventional kagomé-PCF has a FOM_{11} of ~2–10 [13] and (2) ARR-PCFs numerically optimized for HOM suppression offer theoretical FOM_{11} values between 50 and 600 over limited wavelength ranges [14,15]. We also note that in the case of bandgap fibers with hollow leakage channels ("shunts") in the cladding, FOM_{11} values of order 400 can be realized [16]. None of these approaches are, however, free of disadvantages: they either have low FOM, are very difficult to make, offer relatively high LP_{01} mode loss, or do not allow robust single-mode guidance in all wavelength regions where the LP_{01} mode is supported.

Here we report a simple single-ring ARR-PCF design that is scalable and provides very strong HOM suppression within all the low-loss guidance bands of the fiber. Additionally, the structure is characterized by a simple, dimensionless geometrical parameter. All these features may be viewed as mimicking ESM guidance in solid-core PCF. As a convenient shorthand, therefore, we denote this new type of PCF as hESM (hollow-core endlessly single-mode). Note that, for clarity, we will refer to the core modes using the LP_{lm} notation and the modes of the surrounding capillaries using the notation ARE_{lm}, where l and m represent the azimuthal and radial orders of the modes.

The hESM structure consists of a central hollow core (inner diameter D) surrounded by six evenly spaced and nontouching capillaries (AREs) with wall thickness t and inner diameter d (see the left-hand panel in Fig. 1), attached to the inner surface of a thick-walled capillary. We have discovered by finite element (FE) modeling that extremely high values of FOM_{11} (several thousand) can be achieved over all wavelength bands where the fiber guides with low loss, provided the ratio $d/D \approx 0.68$. We provide a physical interpretation for the numerical results using a simple analytical model based on coupled capillary modes. The model readily explains the

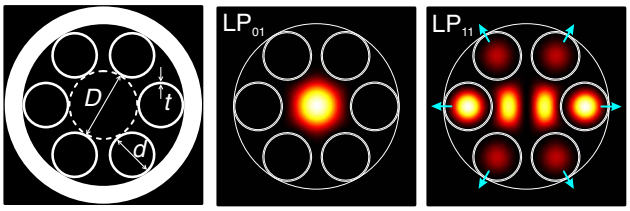

Fig. 1. (a) Sketch of the structure, with the key dimensions marked in core diameter D, inner ARE diameter d, and wall thickness t. (b) Fundamental LP_{01} mode is strongly confined, being antiresonant with modes in the ARE capillaries. (c) Higher-order modes, e.g., the illustrated LP_{11} mode, experience high loss because they are phase-matched to resonances in the AREs. Core light leaks out through the AREs into the solid glass sheath (indicated by the blue arrows). For optimal HOM suppression, $d/D = 0.68$.

importance of the dimensionless parameter d/D. Experimentally, we demonstrate an hESM-PCF with a d/D parameter of 0.64, FOM_{11} of ~96 and broadband guidance windows with losses of the LP_{01} mode at 0.18 dB/m in the vicinity of 1.6 μm. This FOM_{11} is more than 15 × larger than in kagomé-PCF, making the hESM design desirable for applications requiring transmission of $M^2 \sim 1$ beams.

The modal index and loss for the LP_{01} and LP_{11} core modes of a straight hESM-PCF, calculated using FE modeling, are plotted in Fig. 2(a) against the ratio d/D for $t/D = 0.01$ and $D/\lambda = 20$. The glass refractive index n_g was set to a constant value of 1.45 (a good approximation for silica in the range 0.8–1.5 μm), and the hollow regions were taken to be vacuum. For reference, the effective index and loss of the ARE_{01} mode of an isolated capillary in vacuum are also included (brown dashed lines). Figure 2(a) shows that the index of the LP_{01} core mode is high enough to avoid resonant coupling to the ARE_{01}

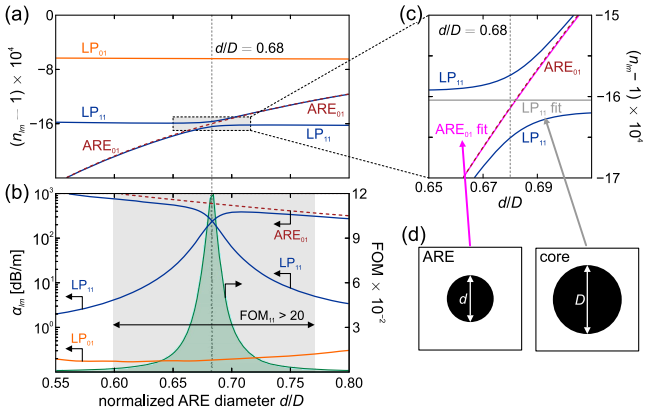

Fig. 2. (a) Modal refractive indices of the LP_{01} (orange) and even and odd LP_{11} (blue) modes. (b) Modal losses and FOM_{11} (green). The brown dashed curves in each plot refer to the ARE_{01} mode of an isolated ARE capillary. The geometrical parameters are $t/D = 0.01$ and $D/\lambda = 20$. The gray-shaded area in (b) shows the region where $FOM_{11} > 20$. (c) Analytical model. Modal indices of the LP_{11} (grey) and ARE_{01} (purple) modes, calculated using the fit in Eq. (1), assuming isolated thick-walled capillaries in each case. Also plotted are the numerically evaluated indices of the hybrid LP_{11}/ARE_{01} modes for the same parameters as Fig. 2(a) [closeup of the gray rectangle]. (d) Infinitely thick-walled capillaries used to approximate the core and AREs in the analytical model [see Eqs. (1) and (2)].

modes, and remains almost independent of d/D, whereas the LP_{11} core mode undergoes a strong anti-crossing with the ARE_{01} mode at $d/D \approx 0.68$. As one moves away from this anti-crossing, the even and odd eigenmodes evolve asymptotically into uncoupled LP_{11} and ARE_{01} modes. Core modes of an even higher order (not shown in Fig. 2) have lower indices and couple to highly leaky modes of the ARE ring, some of which are concentrated in the gaps between the AREs. Figure 2(b) shows the calculated leakage loss of the LP_{01} mode and the hybrid LP_{11}/ARE_{01} modes as a function of d/D. The LP_{01} core mode has a relatively constant loss with a minimum value of 0.17 dB/m at $d/D \approx 0.65$ which is a value similar to that seen in loss optimized annular tubes within a circular jacket [17]. The FOM_{11} increases strongly at the anti-crossing [green curve in Fig. 2(b)], peaking at a value of ~1200. The range where $FOM_{11} > 20$ (i.e., >4 × higher than in kagomé-PCFs [13] with a similar D/λ) is gray shaded in Fig. 2(b) ($0.60 \le d/D \le 0.77$). For a comprehensive analysis of HOM suppression, the FOM of all the higher-order core modes must be calculated. FE modeling reveals that the HOM with the next lowest loss after the LP_{11} mode is the four-lobed LP_{21} mode, with an average FOM_{21} of ~70 at $d/D \approx 0.68$ and an anti-crossing with the ARE_{01} mode at $d/D \approx 0.53$. In experiments, however, this particular mode is less likely to be excited by end-fire illumination or by stress- and bend-induced scattering from the LP_{01} mode (the index difference is some two times higher than for the LP_{11} mode). FE modeling shows that the average FOM_{lm} increases strongly for LP_{lm}-like modes of even higher order (e.g., $FOM_{02} \approx 584$, $FOM_{31} \approx 1446$, and $FOM_{12} \approx 1850$), with the result that they have an insignificant impact on the single-mode performance.

The scalability and broadband guidance of the hESM structure can be illustrated by analyzing the dependence of the modal properties on D/λ. Broadband phase matching between LP_{11} and ARE_{01} modes means that the hESM structure provides robust single-mode guidance at all wavelengths within the LP_{01} transmission window, the width of which is limited by capillary wall resonances (controlled by varying t/D) at shorter wavelengths and by weakening confinement at longer wavelengths [18]. To understand why maximum HOM suppression occurs at $d/D = 0.68$ for all wavelengths, we now present an analytical model in which the core and the AREs are treated as thick-walled capillaries [see Fig. 2(d)]. The modal indices of the LP_{lm} modes in a thick-walled capillary can be approximated by the modified Marcatili–Schmeltzer expression [19]:

$$n_{lm} = \sqrt{1 - \left(\frac{u_{lm}}{\pi f}\right)^2 \left(\frac{\lambda}{d_i}\right)^2}, \quad \textbf{(1)}$$

where u_{lm} is the m-th zero of the Bessel function J_l, and $d_i = d$ or D is the inner diameter of the capillary. The f-parameter is used heuristically to fit the analytical values from Eq. (1) to the results of FE simulations of the core and AREs. It corrects for the noncircular core, the finite wall thickness, and the inhomogeneous environment surrounding the AREs. Figure 2(c) shows the refractive indices of the two LP_{11} and ARE_{01} modes (blue and brown curves, respectively) together with the fitted values for the LP_{11} (gray, zero line) and ARE_{01} (purple curve) modes computed using Eq. (1) with fit parameters $f_{co} = 1.077$ for the core and $f_{ARE} = 0.991$ for the ARE. Analytical and

numerically computed values are in excellent agreement. The convenient analytical form of Eq. (1) allows one to derive a simple expression for the d/D value at which the LP_{11} and ARE_{01} modes couple optimally [18]:

$$\frac{d}{D} = \frac{u_{01}}{u_{11}} \frac{f_{co}}{f_{ARE}} = 0.682. \quad (2)$$

This yields values that agree very well with those obtained from FE modeling [Fig. 2(b)]. Equation (2) provides a convenient rule of thumb for designing robustly single-mode hESM-PCFs. To a first approximation, the design depends neither on the refractive indices nor on the absolute physical dimensions of the fiber, making the design scalable. This means that, provided the ratio d/D is maintained, it is possible to design large-core hESM-PCFs. The dimensionless parameter d/D for hESM is somewhat similar to the well-known d/Λ parameter in solid-core ESM-PCFs. In both fibers, HOMs are strongly suppressed compared to the fundamental mode, and both structures are scalable. We note that Eqs. (1) and (2) can also be used to find structural fiber parameters where other higher-order modes are optimally suppressed. For example, for the almost degenerate LP_{21} and LP_{02} modes, the value of d/D obtained from Eq. (2) is very close to 0.53, which agrees with the optimum value obtained by FE modelling [18].

A hESM-PCF was fabricated using the stack-and-draw technique. First, six capillaries (3.7 mm diameter, 90% air-filling fraction) were stacked in the corners of a jacket tube with a hexagonal inner shape (20 mm flat-to-flat distance). This allowed precise azimuthal positioning of the capillaries at 60° intervals [20]. The preform was then drawn into canes and, subsequently, into a fiber with $D = 30$ μm, $d/D = 0.64$, and $t = 0.44$ μm [a scanning electron micrograph (SEM) is shown in the inset of Fig. 3(a)]. As can be seen, the AREs are almost circular, each having two points of contact with the outer glass sheath. Although the d/D value is not quite optimal, the fiber is still predicted [see Fig. 2(b)] to display much greater HOM suppression than conventional kagomé-PCF.

In a first experiment, broadband supercontinuum (SC) light was launched into a straight 59 cm length of hESM fiber using a microscope objective. The launch was optimized for 620 nm, resulting in ~90% coupling efficiency at this wavelength. The resulting normalized transmission spectrum is plotted in Fig. 3(a), revealing a broad transmission band interrupted by two deep and narrow loss bands, which are caused by anti-crossings between the LP_{01} core mode and the first- and second-order resonances of the ARE walls. The wavelength of the q-th order wall resonance is given to good accuracy by [21]

$$\lambda_q \approx \frac{2t}{q} \sqrt{n_g^2 - 1}, \quad (3)$$

which for $t = 0.44$ μm and $n_g = 1.45$ yields $\lambda_1 = 0.92$ and $\lambda_2 = 0.46$ μm, in very good agreement with the experimental dips at 0.93 and 0.47 μm.

We then tested the guidance properties of a 53 m length of hESM fiber coiled up on a spool of radius 7.5 cm. SC light was launched to the input face of the hESM-PCF, and the transmitted spectrum measured using an optical spectrum analyzer (OSA) and a mid-IR spectrometer.

The loss was then determined using the multiple cutback technique [Fig. 3(b)]. The results show that the guidance band of the coiled fiber extends from 1.17 μm to at least 2.09 μm

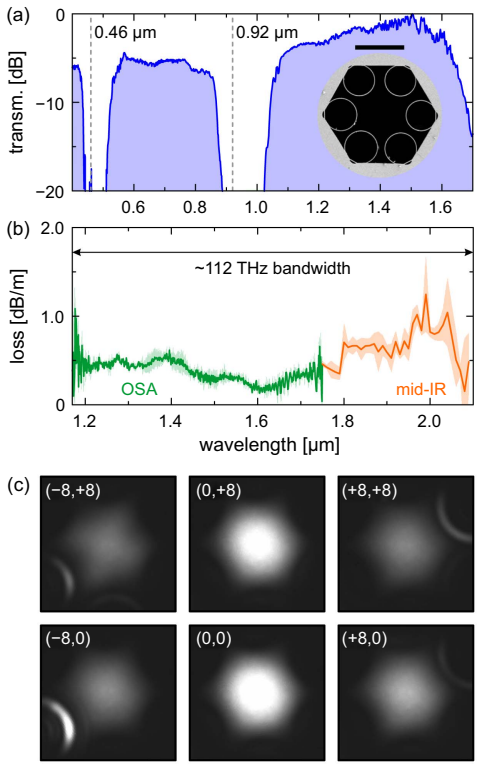

Fig. 3. (a) Transmission of the LP_{01} mode (normalized to the SC spectrum) through a straight 59 cm length of hESM fiber. The vertical dashed lines mark the calculated positions of the first- and second- order resonances at 0.92 and 0.46 μm [see Eq. (3)], and the inset shows an SEM of the hESM-PCF, with parameters $D = 30$ μm, $d/D = 0.64$, and $t = 0.44$ μm. The scale bar corresponds to 25 μm. (b) Measured attenuation through a 53 m long fiber piece, coiled on a spool with 7.5 cm radius. The shaded regions indicate the standard error. (c) Optical near-field images at 1.55 μm ($D/\lambda \approx 19$) for different lateral in-coupling positions; the numbers in parentheses indicate the two-axis transverse displacement in μm.

(~112 THz bandwidth), with a loss of 0.18 ± 0.02 dB/m at 1.6 μm. Compared to typical kagomé-PCF [6,13,22] the loss spectrum is much flatter (~1 dB variation over the entire guidance band), which is of interest for broadband, high-power beam delivery applications. Compared to the straight fiber, the guidance band is narrower, and the transmission bands at shorter wavelength are not seen. We attribute the transmission drop at wavelengths below ~1.2 μm to a mechanism similar to that seen in ESM-PCF [12], where bending transforms the LP_{01} mode into the LP_{11} mode, resulting in high loss: effectively, there is a short-wavelength bend edge. A more detailed analysis of bend sensitivity will be the subject of future work.

To test the robustness and purity of hESM behavior, we butt-coupled a single-mode fiber to a straight 57 cm length of hESM-PCF and explored the effects of lateral misalignment while maintaining constant spacing between the end-faces. The near-field distribution at the output face was tracked using a microscope objective, a 1550 ± 10 nm bandpass filter and a CCD camera. At maximum transmission, i.e., perfect alignment of the fibers, a clean fundamental mode was observed [Fig. 3(c)]. Misalignment caused the launch efficiency of the LP_{01} mode to fall as expected, but no evidence for HOM excitation was found

at any value of lateral misalignment, indicating that the fiber acts as an effective modal filter. Note that at some positions the input beam overlaps with the ARE capillaries, resulting in excitation of modes guided within the thin glass walls; see, for example, the (−8, 0) panel in Fig. 3(b). We attribute the different signal strengths for horizontal and vertical misalignment [for example, see panels (+8, 0) and (0, +8)] to variations in coupling efficiency. Because the LP_{01} mode has different mode field diameters in horizontal and vertical directions [for the parameters of Fig. 3(c), the ratio of horizontal to vertical beam diameters is ∼95.6%], the lateral displacement of a Gaussian beam results in different overlap integrals in these directions.

For a more quantitative assessment of single-mode purity, we used a recently reported prism coupling technique [22] to selectively excite individual HOMs at 1.330 and 1.064 μm (using single-frequency lasers). Figure 4(a) shows the optical near-field images of the first six HOMs at 1.330 μm, excited in a 6 cm

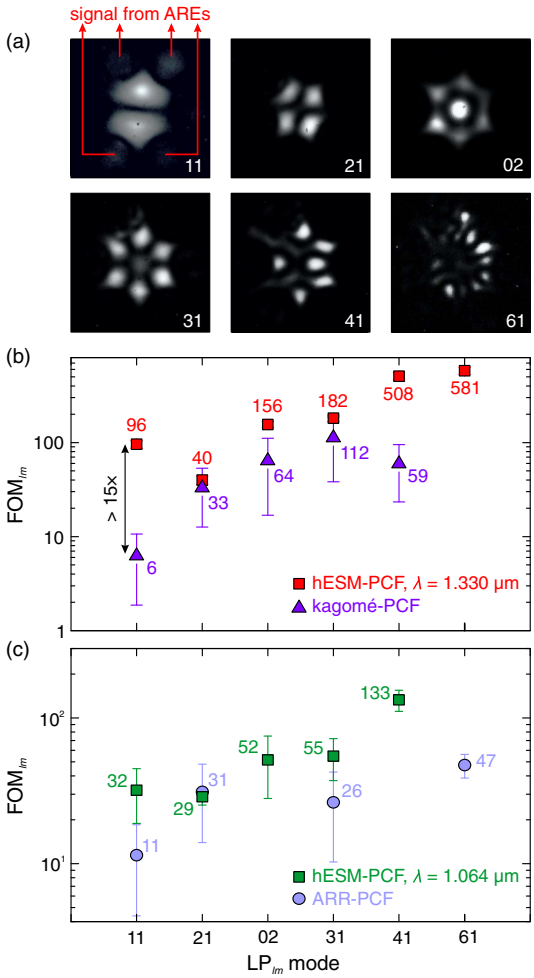

Fig. 4. (a) Optical near-field images at 1.33 μm ($D/\lambda \approx 23$) for the six lowest-order HOMs, obtained using prism coupling into a 6 cm long hESM-PCF [identical fiber to that used in Fig. 3(a)]. Note the expected coupling between ARE_{01} and LP_{11} modes. (b), (c) FOM_{lm} (red and green squares) at (b) 1.330 μm and (c) 1.064 μm ($D/\lambda \approx 28$). The LP_{01} mode loss is (b) 0.46 ± 0.04 dB/m and (c) 2.21 ± 0.02 dB/m, and the bars show the standard error in the FOM values. In (b) the violet triangles show the FOM_{lm} of a kagomé-PCF with $D/\lambda = 26$ [22]. In (c) the blue circles indicate the FOM_{lm} of an ARR-PCF with $d/D = 0.53$ and $D/\lambda = 41$ [20].

length of hESM-PCF. Each image was digitally post-processed to enhance the visibility. When the LP_{11} mode was excited, ARE_{01} light was observed in the capillaries (top left panel), as expected from the discussion above. A similar overall pattern is seen in the FE simulations, although the signal strength in the AREs compared to Fig. 1 (right-hand panel) is somewhat weaker. We attribute this to the non-optimal value of $d/D = 0.64$, which introduces a degree of dephasing between LP_{11} and ARE_{01} modes.

Using prism coupling and cutback, we next measured the loss of individual HOM core modes and directly calculated their FOM values at 1.330 μm. The results are plotted in Fig. 4(b) (red squares). With a value of ∼96, FOM_{11} is more than 15 times larger than its value in kagomé-PCF [22] for similar D/λ ratios [violet triangles in Fig. 4(b)]. The FOM_{21} for the LP_{21} mode was 40, and the FOMs of all the remaining higher-order modes were greater than 155. The measured FOMs at 1.064 μm are shown in Fig. 4(c), together with the values for an ARR-PCF with a non-optimal value of $d/D \approx 0.53$ [20]. For this fiber $FOM_{11} < FOM_{21}$, confirming that tuning the d/D parameter closer to 0.68 does indeed improve suppression of the LP_{11} mode.

REFERENCES

1. J. D. Shephard, J. D. C. Jones, D. P. Hand, G. Bouwmans, J. C. Knight, P. St.J. Russell, and B. J. Mangan, Opt. Express **12**, 717 (2004).
2. P. St.J. Russell, P. Hölzer, W. Chang, A. Abdolvand, and J. C. Travers, Nat. Photonics **8**, 278 (2014).
3. T. Ritari, J. Tuominen, H. Ludvigsen, J. C. Petersen, T. Sørensen, T. P. Hansen, and H. R. Simonsen, Opt. Express **12**, 4080 (2004).
4. A. M. Cubillas, S. Unterkofler, T. G. Euser, B. J. M. Etzold, A. C. Jones, P. J. Sadler, P. Wasserscheid, and P. St.J. Russell, Chem. Soc. Rev. **42**, 8629 (2013).
5. N. M. Litchinitser, S. C. Dunn, B. Usner, B. J. Eggleton, T. P. White, R. C. McPhedran, and C. M. de Sterke, Opt. Express **11**, 1243 (2003).
6. F. Benabid, J. C. Knight, G. Antonopoulos, and P. St.J. Russell, Science **298**, 399 (2002).
7. A. D. Pryamikov, A. S. Biriukov, A. F. Kosolapov, V. G. Plotnichenko, S. L. Semjonov, and E. M. Dianov, Opt. Express **19**, 1441 (2011).
8. W. Belardi and J. C. Knight, Opt. Express **22**, 10091 (2014).
9. A. Hartung, J. Kobelke, A. Schwuchow, J. Bierlich, J. Popp, M. A. Schmidt, and T. Frosch, Opt. Lett. **40**, 3432 (2015).
10. A. N. Kolyadin, A. F. Kosolapov, A. D. Pryamikov, A. S. Biriukov, V. G. Plotnichenko, and E. M. Dianov, Opt. Express **21**, 9514 (2013).
11. F. Yu, W. J. Wadsworth, and J. C. Knight, Opt. Express **20**, 11153 (2012).
12. T. A. Birks, J. C. Knight, and P. St.J. Russell, Opt. Lett. **22**, 961 (1997).
13. T. G. Euser, G. Whyte, M. Scharrer, J. S. Y. Chen, A. Abdolvand, J. Nold, C. F. Kaminski, and P. St.J. Russell, Opt. Express **16**, 17972 (2008).
14. F. Poletti, Opt. Express **22**, 23807 (2014).
15. C. Wei, R. A. Kuis, F. Chenard, C. R. Menyuk, and J. Hu, Opt. Express **23**, 15824 (2015).
16. J. M. Fini, J. W. Nicholson, R. S. Windeler, E. M. Monberg, L. Meng, B. Mangan, A. DeSantolo, and F. V. DiMarcello, Opt. Express **21**, 6233 (2013).
17. F. Poletti, J. R. Hayes, and D. J. Richardson, *37th European Conference and Exposition on Optical Communications* (Optical Society of America, 2011).
18. M. C. Günendi, P. Uebel, M. H. Frosz, and P. St.J. Russell, arXiv:1508.06747 [physics.optics] (2015).
19. E. A. J. Marcatili and R. A. Schmelzter, Bell Syst. Tech. J. **43**, 1783 (1964).
20. N. N. Edavalath, M. H. Frosz, J.-M. Ménard, and P. St.J. Russell, *Frontiers on Optics* (Optical Society of America, 2015).
21. J.-L. Archambault, R. J. Black, S. Lacroix, and J. Bures, J. Lightwave Technol. **11**, 416 (1993).
22. B. M. Trabold, D. Novoa, A. Abdolvand, and P. St.J. Russell, Opt. Lett. **39**, 3736 (2014).